Gaining Insight into the Role of the Solvent during Spray Drying of Amorphous Solid Dispersions by Studying Evaporation Kinetics br

DOI: 10.1021/acs.molpharmaceut.2c00095
Handle: http://hdl.handle.net/1942/37577

Gaining insight in the role of the solvent during spray drying of amorphous solid dispersions by studying evaporation kinetics

Sien Dedroog[a], Peter Adriaensens[b] and Guy Van den Mooter[a*]

[a] *Drug Delivery and Disposition, KU Leuven, Department of Pharmaceutical and Pharmacological Sciences, Campus Gasthuisberg ON2, Herestraat 49 b921, 3000 Leuven, Belgium*

[b] *Applied and Analytical Chemistry, Institute for Materials Research, Hasselt University, Agoralaan 1-Building D, 3590 Diepenbeek, Belgium*

[*] *Corresponding author:*

Guy Van den Mooter; Drug Delivery and Disposition, KU Leuven, Department of Pharmaceutical and Pharmacological Sciences, Campus Gasthuisberg ON2, Herestraat 49 b921, 3000 Leuven, Belgium
Guy.vandenmooter@kuleuven.be; Tel.: +32 16 330304

Graphical abstract/Table of contents only

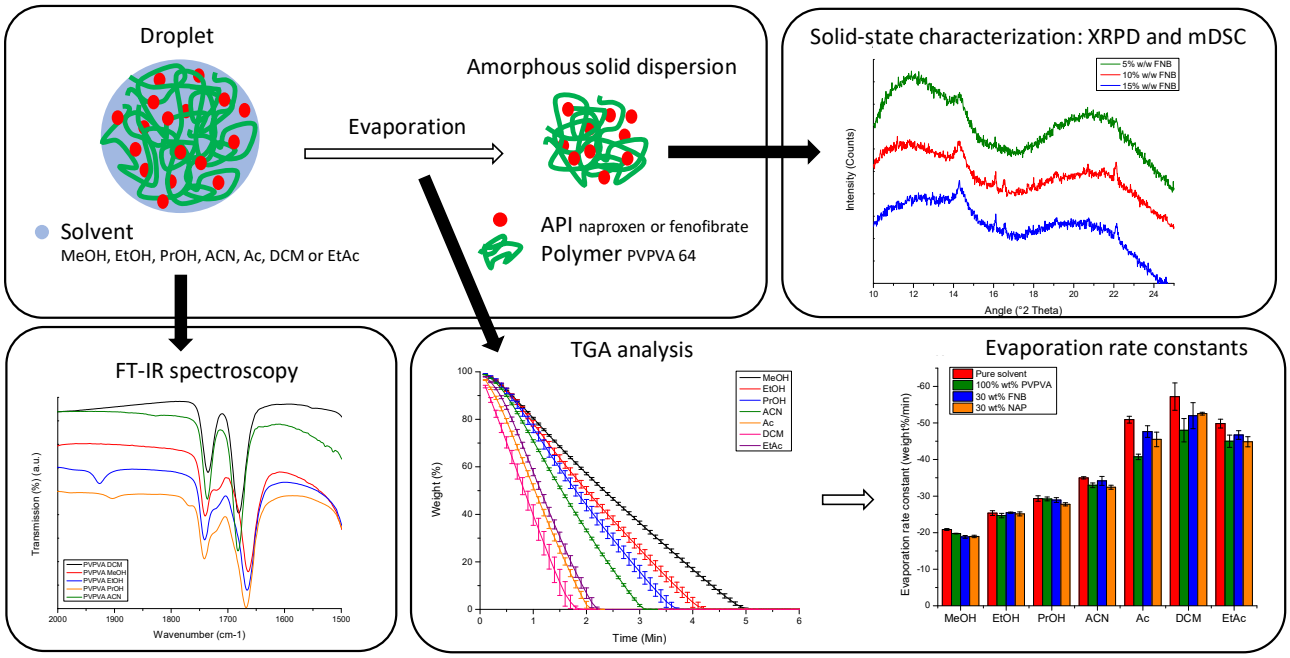

Abstract

Spray drying is one of the most commonly used manufacturing techniques for Amorphous Solid Dispersions (ASDs). During spray drying, very fast solvent evaporation is enabled by the generation of small droplets and exposure of these droplets to a heated drying gas. This fast solvent evaporation leads to an increased viscosity that enables kinetic trapping of an Active Pharmaceutical Ingredient (API) in a polymer matrix, which is favorable for the formulation of supersaturated, kinetically stabilized ASDs. In this work, the relation between the solvent evaporation rate and the kinetic stabilization of highly drug loaded ASDs was investigated. Accordingly, Thermal Gravimetric Analysis (TGA) was employed to study the evaporation kinetics of seven organic solvents and the influence of solutes, *i.e.,* poly(vinylpyrrolidone-*co*-vinyl acetate) (PVPVA), fenofibrate (FNB) and naproxen (NAP), on the evaporation behavior. At 10 °C below the boiling point of the respective solvent, methanol (MeOH) had the lowest evaporation rate and dichloromethane (DCM) the highest. PVPVA decreased the evaporation rate for all solvents, yet this effect was more pronounced for the relatively faster evaporating solvents. The APIs had opposite effects on the evaporation process: FNB increased the evaporation rate, while NAP decreased it. The latter might indicate the presence of interactions between NAP and the solvent or NAP and PVPVA, which was further investigated using Fourier Transform – InfraRed (FT-IR) spectroscopy. Based on these findings, spray drying process parameters were adapted to alter the evaporation rate. Increasing the evaporation rate of MeOH and DCM enabled the kinetic stabilization of higher drug loadings of FNB, while the opposite trend was observed for ASDs of NAP. Even when higher drug loadings could be kinetically stabilized by adapting the process parameters, the improvement was limited, demonstrating that the phase behavior of these ASDs of FNB and NAP immediately after preparation was predominantly determined by the API-polymer-solvent combination rather than the process parameters applied.

Keywords: *Amorphous solid dispersions – Spray drying – Solvent – Evaporation – Interactions – Fenofibrate – Naproxen*

Abbreviations

Ac	Acetone
ACN	Acetonitrile
API	Active Pharmaceutical Ingredient
ASDs	Amorphous Solid Dispersions
Bp	Boiling point
DCM	Dichloromethane
EtAc	Ethyl acetate
EtOH	Ethanol
FNB	Fenofibrate
FT-IR	Fourier Transform InfraRed spectroscopy
GFA	Glass Forming Ability
mDSC	Modulated Differential Scanning Calorimetry
MeOH	Methanol
NAP	Naproxen
PrOH	Isopropanol
PVPVA	Poly(vinylpyrrolidone-*co*-vinyl acetate)
TGA	Thermal Gravimetric Analysis
T_{in}	Inlet temperature
T_{out}	Outlet temperature
XRPD	X-Ray Powder Diffraction

1. Introduction

Spray drying is widely applied for the manufacturing of Amorphous Solid Dispersions (ASDs), which are molecular dispersions of an Active Pharmaceutical Ingredient (API) in a polymer matrix at solid state[1]. The spray drying procedure starts with dissolving the API together with its carrier in a common solvent, which is subsequently atomized into droplets inside the drying chamber, where heat is transferred towards the droplet surface and solvent evaporation occurs. The very fast solvent evaporation gives rise to a fast increase in viscosity, which is a critical factor for kinetic trapping of an API in a polymer matrix and might result in kinetic stabilization of supersaturated molecular dispersions[2]. Generally, the higher the solvent drying rate, the higher the chance at kinetic trapping and thus the formation of supersaturated/highly drug loaded ASDs. Accordingly, it has been reported that the solvent evaporation rate was an even more important factor than the polymer molecular weight and the drug to polymer ratio to decrease the extent of nucleation in ASDs[3].

There are several factors that could influence the drying rate, such as droplet size, physicochemical properties of the solutes, drying gas temperature and especially the type of solvent that is employed[2]. For spray drying, the solvent should measure up to the following criteria: have a common solubilizing capacity for API and polymer (and other additives), an acceptable viscosity, a low toxicity, a high volatility, be non-combustive and the solutes should have an acceptable chemical stability in solution[4]. Although selecting a solvent in which all compounds have a sufficiently high solubility is critical, it was found in previous work that the importance of the solubility for the phase behavior of ASDs should not be overestimated[5]. More specifically, the solvent determined the amount of API that could be kinetically stabilized in the poly(vinylpyrrolidone-*co*-vinyl acetate) (PVPVA) matrix immediately after preparation, yet there was no relation between this amount and the equilibrium solubility of the API in the respective solvent. Therefore, a molecular level understanding of the interactions between API, polymer and solvent and the resulting physical state of ASDs is of utmost importance to identify additional solvent selection criteria. Accordingly, several authors have been investigating the influence of the solvent on various physicochemical properties of ASDs[6–11]. In view of the formulation of highly drug loaded ASDs, the impact of the solvent on the evaporation behavior is especially important. The tendency to evaporate*, i.e.,* volatility, is reflected by the boiling point (bp) of a solvent, which is the temperature at which the vapor pressure of the solvent is equal to the atmospheric pressure and thus the temperature at which the liquid will start to vaporize. The higher the bp, the lower the vapor pressure at Room Temperature (RT) and thus the less volatile the solvent will be. Not only the temperature, but also the amount of energy that is required for the liquid to gas transition influences the evaporation behavior, which is represented by the heat of vaporization. Moreover, type and

concentration of solutes can also have an impact on the drying process. The presence of solutes will increase the thermal efficiency of the drying process as there is relatively less solvent present that needs to be evaporated[2]. On the other hand, as the presence of solutes increases the entropy in solution, the vapor pressure will be lower, resulting in an increased bp of the solution compared to the pure solvent. Accordingly, the concentration dependent influence of PVP on the evaporation rate of diverse combinations of methanol (MeOH), acetone (Ac) and dichloromethane (DCM) was demonstrated by Paudel et al[9]. Also Al-Obaidi et al. investigated the evaporation behavior of polymer solutions in Ac/water or Ac/MeOH and related it to the viscosity, polymer conformation and relaxation behavior of ASDs of griseofulvin[6]. Likewise, Mugheirbi et al. studied the impact of the water content on the evaporation behavior of DCM combined with different alcoholic solvents and related it to the physical state of ASDs[12]. Also Na Li et al. demonstrated that the presence of a small fraction of water in the solvent mixture could result in phase separation of ASDs of ritonavir and PVPVA[13]. Moreover, the interplay between the solvent evaporation rate and diffusional motion of the solutes in the specific solvent determines the particle morphology of the spray dried particles[14]. As the relation between solution properties and the particle formation process has been extensively studied[15], this work focused on the influence of the solvent evaporation rate on the kinetic stabilization of highly drug loaded ASDs.

Accordingly, the evaporation kinetics of seven single organic solvents, *i.e.*, MeOH, ethanol (EtOH), isopropanol (PrOH), acetonitrile (ACN), Ac, DCM, and ethyl acetate (EtAc), were investigated by means of Thermal Gravimetric Analysis (TGA). These solvents were selected as it was demonstrated in previous work that their different polarity and volatility could give rise to a diverse phase behavior of ASDs[5]. The influence of compounds that dissolve in/mix with the solvent on the evaporation behavior was also of interest: PVPVA, fenofibrate (FNB) and naproxen (NAP) and combinations of these APIs with PVPVA were studied. The structural formulas of these compounds can be found in Fig 1. NAP was selected as it can hydrogen bond with PVPVA: its carboxylic acid group can act as a hydrogen donor for the carbonyl group of PVPVA[16,17]. In contrast, FNB has no hydrogen bonding potential with PVPVA as it has no hydrogen donor groups[18]. However, it was found that the solvent had a large impact on the physical state of ASDs of FNB, with the maximum amount of drug that could be kinetically stabilized ranging from 5 wt% using MeOH to 25 wt% using Ac/EtAc[5]. Besides the expected effect of the solutes on the vapor pressure, also interactions between API-polymer-solvent could interfere with the evaporation process[9]. From the selected solvents, the alcoholic ones are hydrogen bond donors and acceptors, while Ac and EtAc could only act as hydrogen bond accepting solvents. Hence, the prevalence of API-polymer interactions might depend on the solvent in which they are dissolved, which was investigated using Fourier Transform – InfraRed (FT-IR) spectroscopy. In Fig 1, the functional groups for which vibration bands could be detected in the spectral region of 1800 to 1600 cm^{-1} are indicated.

After extensively studying the evaporation kinetics and interactions in solution, the aim of this work was to rationally select new process parameters for spray drying. The potential impact of process parameters on the physical state of ASDs has been extensively described in literature[2,4,15,19–21]. In this study, the parameters were selected in order to adapt the evaporation rate to generate even more supersaturated ASDs. Accordingly, the inlet temperature (T_{in}) was adapted together with the liquid feed rate to modify the droplet size. Ultimately, the kinetic trapping potential was evaluated by demonstrating the potential impact of process optimization on the phase behavior of ASDs of NAP and FNB.

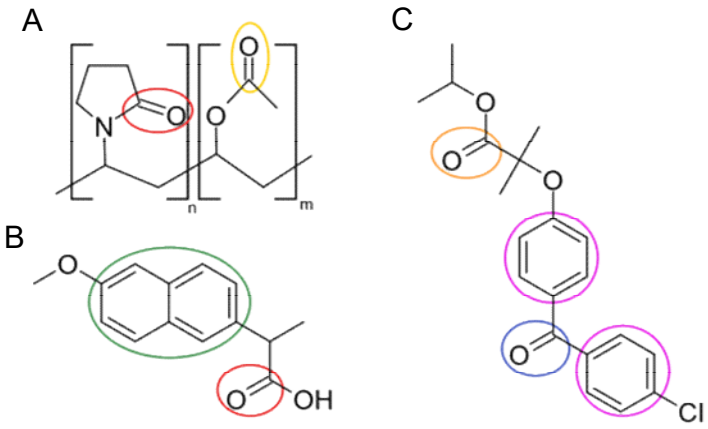

***Figure 1**. Structural formulas of PVPVA (A), NAP (B) and FNB (C). Both the carbonyl stretching vibration of the vinyl pyrrolidone carbonyl (red) and the vinyl acetate one (yellow) could be detected using FT-IR in the spectral region of 1800 to 1600 cm^{-1} (A). For NAP, the carbonyl stretching vibration (red) and aromatic skeleton stretching (green) could be detected (B). For FNB, two carbonyl stretching vibrations (blue, orange) and aromatic skeleton stretching (purple) could be detected (C).*

2. Materials and methods

2.1. Materials

Naproxen (NAP) (PubChem CID: 156391) was obtained from SA Fagron NV (Waregem, Belgium) and fenofibrate (FNB) (PubChemCID: 3339) was purchased from Hangzohou Dayangchem Co. (Hangzhou City, China). Poly(vinylpyrrolidone-*co*-vinyl acetate) 64 (PVPVA 64, Kollidon® VA64) (PubChem CID: 270885) was supplied by BASF® ChemTrade GmbH (Ludwigshafen, Germany).

ACROS Belgium (Geel, Belgium) supplied Methanol (MeOH) (≥ 99.8%) and Sigma-Aldrich (Brussels, Belgium) provided ethyl acetate (EtAc) (≥ 99.5%). Acetone (Ac) (≥ 99%) was received from VWR Chemicals (Leuven, Belgium), denaturated ethanol (EtOH) (≥ 97% and 3% V/V diethylether) from Chem-Lab Analytical (Zedelgem, Belgium) and 2-propanol (PrOH) (≥ 99.9%) from Carl Roth GmbH (Karlsruhe, Germany). Both acetonitrile (ACN) (≥ 99.9%) and dichloromethane (DCM) (≥ 99.5%) were purchased from Fisher Scientific (Loughborough, UK). Molecular sieve (type 4 Å, mesh 8 – 12) was obtained from Sigma-Aldrich (Brussels, Belgium).

2.2. Thermal gravimetric analysis (TGA)

2.2.1. Evaporation kinetics

To study the evaporation kinetics of the seven organic solvents as such (*i.e.,* MeOH, EtOH, PrOH, ACN, Ac, DCM, EtAc), solutions of PVPVA and solutions of PVPVA together with either FNB or NAP a thermogravimetric analyzer TGA 550 (TA instruments, Leatherhead, UK) was used. For the solutions, the solid content was kept constant at 10% w/V, which consisted of either 100 wt% PVPVA or 30 wt% of API and 70 wt% of PVPVA. To investigate the influence of a higher concentration of PVPVA on the evaporation rate of MeOH and DCM, solutions of 30% w/V PVPVA were prepared for these solvents as well. For every analysis, 40 µL of the sample was pipetted directly in a platinum HT pan (TA instruments, Zellik, Belgium) and kept isothermal for 10 min at a temperature 10 °C below the boiling point of the respective solvent. Every sample was analyzed in triplicate.

The recorded weight loss as a function of time was attributed to solvent evaporation, from which the evaporation rate could be determined. In the case of the pure solvents, the evaporation followed a linear behavior, or in other words zero order kinetics, hence the following equation (Eq. 1.) could be employed:

$$y = a + bx \qquad \textit{Equation 1.}$$

Here, y corresponds to the weight (weight%) and x to the time (min). From this, the evaporation rate constant, b (weight%/min), could be established.

For the solutions, the first part of the curve also showed a linear relation, however, it was followed by an exponential decay in weight%, hence, the evaporation followed first order kinetics. The first part of the curve could be described by Eq. 1., while for the second part, a biexponential decay function (Eq. 2.) was applied:

$$y = y_0 + A_1 e^{-x/t1} + A_2 e^{-x/t2} \qquad \textit{Equation 2.}$$

From the time constants (t_1 and t_2, min), the evaporation rate constants (k_1 and k_2) could be deducted. These evaporation rate constants were equal to the reciprocal of the time constants (k_1 and k_2, min^{-1}).

To divide the evaporation behavior into these two parts, the second derivative of the weight change in function of time was used. This allowed the maximal change of the evaporation rate to be established, at which point the curve was divided into two. To exemplify, the division of the evaporation curve for MeOH from a solution containing 10% w/V PVPVA is shown in Fig 2. The curve was split into two at 4.4 min, which was the peak maximum. Before this point, a linear fit was used to determine the evaporation rate constant, and after this maximum, the biexponential decay fit allowed to establish the two evaporation constants that described the last part of the curve.

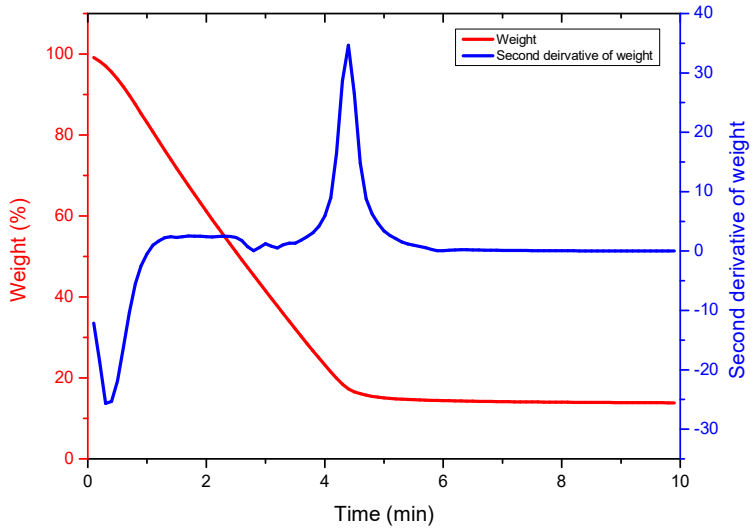

Figure 2. *Weight loss in function of time (red) and its second derivative (blue). The peak maximum in the second derivative was used to divide the curve into a linear and an exponential zone.*

2.2.2. Residual solvent

To determine the amount of residual solvent in the spray dried ASDs after secondary drying, a thermogravimetric analyzer TGA 550 (TA instruments, Leatherhead, UK) was employed as well. Approximately 5 to 10 mg of sample was accurately weighed in a platinum HT pan (TA instruments, Zellik, Belgium) and heated at 5 °C/min to 130 °C. Every batch was analyzed in triplicate. The recorded

weight change as a function of temperature was attributed to solvent evaporation and could be determined using the Universal Analysis software (Version 5.5, TA instruments, Leatherhead, UK).

2.3. Fourier transform – infrared spectroscopy (FT-IR)

Prior to FT-IR analysis, all organic solvents were dried overnight using a molecular sieve type 4 Å to remove residual water present in the solvents. Additionally, PVPVA was dried for 4 days at 60 °C to remove the excess of water present. Solutions of PVPVA (10% w/V), FNB (2% w/V), NAP (2% w/V), PVPVA together with FNB (10% w/V) and PVPVA together with NAP (10% w/V) in MeOH, EtOH, PrOH, ACN and DCM were investigated. For the solutions of PVPVA and a drug compound, the following drug loadings were prepared: 10, 20 and 30 wt% of drug. The organic solvents were also analyzed as such. FT-IR spectra were recorded using a Perkin Elmer Spectrum two by accumulating 16 scans with a resolution set at 1 cm^{-1} over a spectral region of 4000 to 1100 cm^{-1}. The region of interest was the carbonyl stretching vibration region (1800 - 1600 cm^{-1}). For the blank, a background spectrum was recorded and subtracted from the sample spectrum. For every sample, 30 µL was pipetted in a semi demountable cell equipped with CaF_2 cell windows. After the FT-IR analysis in solution, the CaF_2 cell windows were opened, and the sample was dried at RT for 1 min. Subsequently, the dried film was analyzed again to compare the interaction behavior of drug and polymer in solution to that in the dried state. All spectra were analyzed using the OriginPro software (Version 8.5, Northampton, United States).

2.4. Manufacturing of amorphous solid dispersions by spray drying

The drug and polymer were dissolved together in either MeOH or DCM in order to obtain a solid content of 10% w/V. The drug to polymer ratios were dependent on the highest amount of the APIs that could be kinetically stabilized in the PVPVA matrix, which was reported in previous work[5]. For FNB, 5, 10 and 15 wt% of FNB were investigated when using MeOH as a solvent, while in the case of DCM, 20, 25 and 30 wt% of FNB were prepared. For NAP, higher drug loadings of 40 and 45 wt% were studied using MeOH and 45 and 50 wt% of NAP when using DCM. These solutions were spray dried using a Büchi mini spray dryer B-190 (Büchi, Flawil, Switzerland) by applying a drying air flow rate of 33 m^3/h and an atomization air flow rate of 10 L/min. The drying air temperature and feed solution flow rate were adapted, depending on the need for a faster or slower evaporation process. The investigated sets of process parameters are described in Table 1. The ASDs were further dried in a vacuum oven (Mazzali Systems, Monza, Italy) for 4 days at 25 °C, analyzed using XRPD, mDSC and TGA and stored at -28 °C in the presence of phosphorus pentoxide.

Table 1. *Spray drying process parameters per tested condition and per solvent.*

Conditions	Parameters	MeOH	DCM
Higher evaporation rate	Inlet temperature (°C)	85	59
	Feed solution flow rate (mL/min)	2.5	2.5
Standard conditions	Inlet temperature (°C)	65	39
	Feed solution flow rate (mL/min)	5	5
Lower evaporation rate	Inlet temperature (°C)	-	29
	Feed solution flow rate (mL/min)	-	10

2.5. Solid-state characterization of amorphous solid dispersions

2.5.1. Modulated differential scanning calorimetry (mDSC)

A Q2000 mDSC (TA Instruments, Leatherhead, UK) was used to investigate the thermal properties of the spray dried ASDs of NAP. The system was equipped with a Refrigerated Cooling System (RCS 90) and a dry nitrogen purge at 50 mL/min and calibrated for temperature, enthalpy and heat capacity using indium and sapphire standards. Approximately 1 to 5 mg was accurately weighed into aluminum DSC pans (TA instruments, Zellik, Belgium), which were then closed using the corresponding lids (TA instruments, Zellik, Belgium). The samples were heated from -15 °C to 180 °C using a linear heating rate of 2 °C/min combined with a modulation amplitude of 0.212 °C and a period of 40 s. The Universal Analysis software (Version 5.5, TA Instruments, Leatherhead, UK) was used to analyze the thermograms. The T_gs were measured at half height of transition in the reversing heat flow and the T_g width was established by determining the start- and endpoint of the T_g using the derivative of the reversing heat flow. The crystallinity percentages were calculated based on the heat of fusion of pure naproxen (156.1 J/g), thereby taking into account the drug loading that was used.

2.5.2. X-ray powder diffraction (XRPD)

The physical state of the ASDs of both FNB and NAP was investigated using an X'Pert PRO diffractometer (PANalytical, Almelo, the Netherlands) with a Cu tube (Kα λ = 1.5418 Å). The generator was installed at 40 mA and 45 kV. The samples were placed in between two Kapton® Polyimide Thin-films (PANalytical, USA) and continuously scanned from 10 to 25 °2θ. The counting time was installed at 800 s, the step size at 0.0167° and the spinning was set at 4 s/revolution. The obtained diffractograms were analyzed using the X'Pert Data Viewer (Version 1.9a, PANalytical, Almelo, the Netherlands).

2.5.3. Solid state NMR (ssNMR)

High-resolution ^{13}C-CPMAS solid-state NMR

Solid-state ^{13}C-CPMAS (Cross Polarization Magic Angle Spinning) NMR spectra were acquired on a Bruker 400MHz spectrometer (9.4 Tesla) equipped with a 4 mm probe. Magic angle spinning was performed at 10 kHz in ceramic zirconia rotors. The aromatic signal of hexamethylbenzene was used to calibrate the carbon chemical shift scale (132.1 ppm). Acquisition parameters used were: a spectral width of 50 kHz, a 90° pulse length of 4.0 μs, an acquisition time of 15 ms, a recycle delay time of 2.5 s, a spin-lock field of 50 kHz, a contact time of 2 ms and between 25000 and 60000 accumulations. High power proton dipolar decoupling during acquisition was set to 70 kHz.

^{13}C liquid-state NMR

The ^{13}C-NMR spectrum of Fenofibrate was measured at room temperature on a 400 MHz Varian Inova NMR spectrometer using a 5 mm OneNMR PFG probe. Hereto a solution of 130 mg/ml crystalline Fenofibrate was prepared $CDCl_3$ supplemented with 15mM $Cr(acac)_3$ as relaxation reagent. The chemical shift scale (δ; in ppm) was calibrated relatively to $CDCl_3$ (77.7 ppm). All spectra were acquired with a 90° pulse of 8.0 μs, a spectral width of 27.8 kHz, an acquisition time of 1 s, a relaxation delay of 6 s and 8000 accumulations. A line-broadening of 3 Hz was applied prior to Fourier transformation to the frequency domain.

3. Results

3.1. Evaporation kinetics

3.1.1. Evaporation kinetics of pure organic solvents

The evaporation behavior of the seven organic solvents was determined by recording the weight loss over time at 10 °C below the boiling point of the respective solvent. From Fig 3A, it was clear that the slope of the weight loss curve in function of time was steepest for DCM, while it was flattest for MeOH. In Fig 4A, the corresponding evaporation rate constants determined using a linear fit (Eq. 1.) are shown.

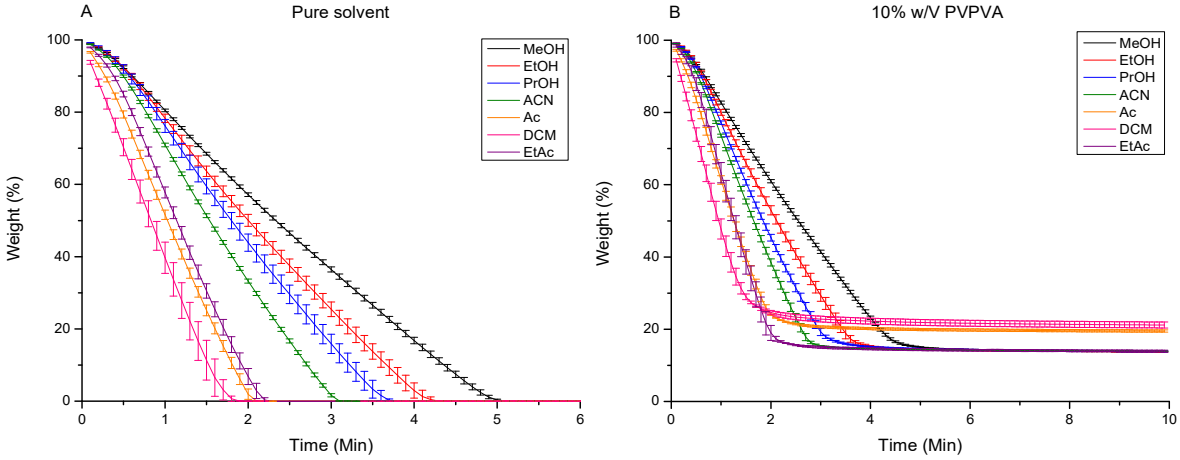

***Figure 3**. Weight loss in function of time of pure solvents (A) and solutions containing 10% w/V PVPVA (B) when kept isothermal at 10 °C below the boiling point of the respective solvent. The following color code was applied: MeOH in black, EtOH in red, PrOH in blue, ACN in green, Ac in orange, DCM in pink and EtAc in purple.*

3.1.2. The influence of PVPVA on the evaporation kinetics

Solutions containing 10% w/V PVPVA had the same relative evaporation behavior as the pure organic solvents (Fig 3B). However, for all solvents (except for PrOH), PVPVA slowed down the evaporation process (Fig 4A), which was most pronounced for the faster evaporating solvents, *i.e.*, DCM, Ac and EtAc. The final weight% in case of DCM and Ac was slightly higher compared to the other solvents (Fig 3B), which indicated that more DCM and Ac was already evaporated before the start of the TGA analysis. To confirm the different impact of PVPVA on the evaporation rate of relatively faster and slower evaporating solvents, the evaporation behavior of solutions of 30% w/V PVPVA in MeOH, *i.e.,* the slowest evaporating solvent, and DCM, *i.e.,* the fastest one, was investigated. In Fig 5, the corresponding drying rate constants are reported. It was clear that 30% w/V of PVPVA immediately reduced the rate of volatilization of DCM by ca. 50%, while it initially had no effect on the evaporation of MeOH (Fig 5A). Further progress of the evaporation behavior showed similar evaporation rate constants for MeOH and DCM for the second part of the curve (Fig 5B, C).

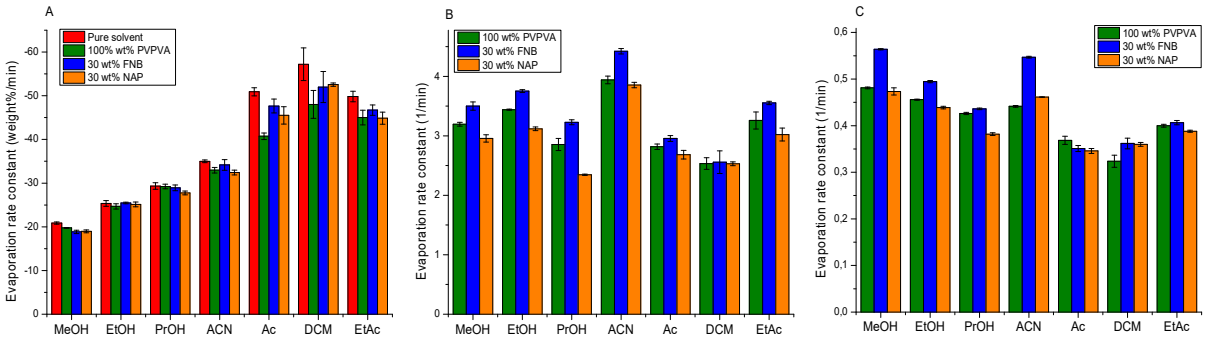

293

294 ***Figure 4.*** *Evaporation rate constants determined from the weight loss as a function of time using a linear fit (A) and a*
295 *subsequential biexponential fit (B, C). The following color code was applied: pure solvents in red, solutions only containing*
296 *PVPVA in green, the ones containing both PVPVA and FNB in blue and the ones comprising both PVPVA and NAP in orange.*

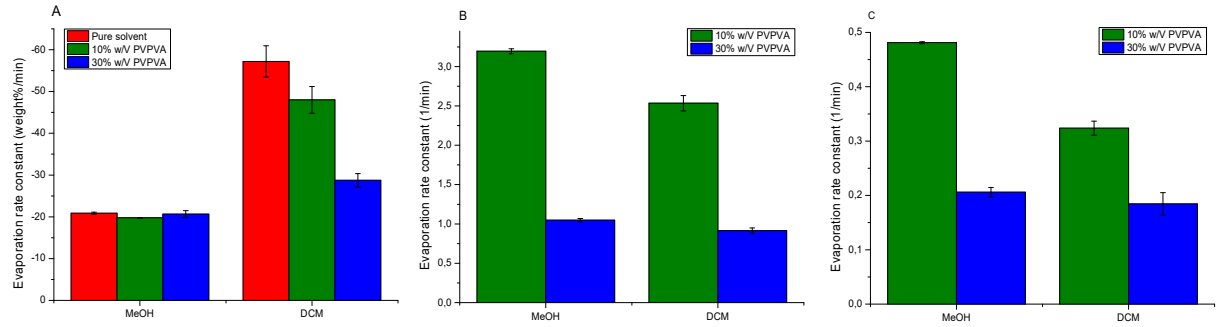

297

298 ***Figure 5****. Evaporation rate constants determined from the weight loss as a function of time using a linear fit (A) and a*
299 *subsequential biexponential fit (B, C). The constants for pure MeOH and DCM are shown in red, those of solutions containing*
300 *10% w/V PVPVA in green and the ones with 30% w/V PVPVA in blue.*

301 3.1.3. The influence of drug compounds on the evaporation kinetics

302 In Fig 4, the effect of either 30 wt% FNB or 30 wt% NAP on the evaporation behavior is depicted.
303 Initially, the evaporation rate of DCM, Ac and EtAc was increased in case of the 30 wt% drug solutions
304 compared to the ones solely containing PVPVA (Fig 4A). Further in time, the evaporation rate constants
305 for 30 wt% FNB solutions were highest, followed by the 100 wt% PVPVA solutions and at last the 30
306 wt% NAP solutions, independently of the solvent, with as an exception DCM (Fig 4B). Later, the same
307 trend was still observed in case of MeOH, EtOH, PrOH and EtAc, yet not anymore in the case of the
308 other solvents (Fig 4C).

309 **3.2. FT-IR spectroscopy**

310 3.2.1. The behavior of PVPVA, NAP and FNB in solution

311 In Fig 6A, the different behavior of 10% w/V PVPVA in DCM, ACN, MeOH, EtOH and PrOH is depicted.
312 The exact peak positions depending on the solvent are described in Table S1 in Supplementary
313 information. For DCM, the first signal, *i.e.*, 1735 cm^{-1}, corresponds to the carbonyl stretching vibration
314 of vinyl acetate (VA) (marked in yellow in Fig 1A), while the second one, *i.e.*, 1681 cm^{-1}, originated from

the carbonyl stretching vibration of vinyl pyrrolidone (VP) (marked in red in Fig 1A)[22,23]. PVPVA behaved similarly when dissolved in ACN, while its behavior clearly differed in the alcoholic solvents. Here, the carbonyl stretching signal of VA was split in a non-hydrogen bonded vibration signal, which was situated at higher wavenumbers, and a hydrogen bonded vibration signal, which was positioned at lower wavenumbers. Additionally, the signal corresponding to the VP carbonyl stretching vibration was broadened and shifted towards lower wavenumbers. The peak shift of the VP stretching vibration was dependent on the alcoholic solvent in which PVPVA was dissolved, with the largest shift in the case of MeOH (*i.e.,* 1664 cm^{-1}), followed by EtOH (*i.e.,* 1666 cm^{-1}) and the smallest in PrOH (*i.e.,* 1668 cm^{-1}).

A well-known property of naproxen is that it can self-associate and form both dimers and open-chain oligomers[16,24,25]. In case of DCM, the first signal corresponded to the carbonyl stretching vibration of the monomer, *i.e*., 1748 cm^{-1}, while the second one correlated to that of the dimer, *i.e.,* 1710 cm^{-1} (marked in red in Fig 1B) (Table S1 in Supplementary info). The other two signals in this spectral region originated from aromatic skeleton stretching vibration, namely, in plane C-H bending at 1636 cm^{-1} and in plane C-C stretching at 1607 cm^{-1} (marked in green in Fig 1B)[25]. In ACN, only the carbonyl stretching vibration corresponding to the NAP monomer (*i.e.,* 1740 cm^{-1}) was observed, and in case of the three alcoholic solvents NAP manifested itself as both monomer (*i.e.,* 1738 cm^{-1}) and dimer (*i.e*., 1708 cm^{-1}), although there was relatively less dimer present when compared to DCM (Fig 6B)[16].

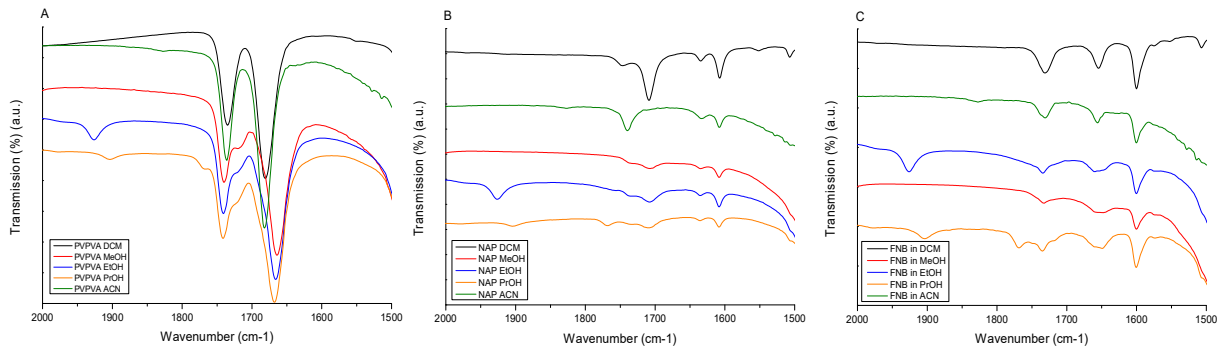

Figure 6. *FT-IR spectra of 10% w/V PVPVA (A), 2% w/V NAP (B) and 2% w/V FNB (C) in DCM (black), ACN (green), MeOH (red), EtOH (blue) and PrOH (orange). The transmittance is depicted in arbitrary units.*

The behavior of FNB in the organic solvents is depicted in Fig 6C and the corresponding peak positions per solvent in Table S2 in Supplementary information. The first peak correlated to the carbonyl stretching vibration of the ester carbonyl, *i.e.,* 1732 cm^{-1} (indicated in orange in Fig 1C), the second one to the other carbonyl stretching vibration signal, *i.e.,* 1654 cm^{-1} (marked in blue in Fig 1C), and the last signal detected in this spectral region corresponded to the in-plane benzene ring stretch, *i.e.,* 1600 cm^{-1} (indicated in purple in Fig 1C)[26]. FNB showed similar behavior in DCM and ACN, but in the other three solvents the second carbonyl stretching vibration signal was broadened.

3.2.2. The presence of interactions between NAP and PVPVA in solution

After characterization of the reference compounds in solution, solutions of different API to polymer ratios were characterized to investigate possible interactions between API and polymer and the impact of the solvent on the prevalence of these interactions.

In Fig 7, the IR spectra of solutions containing 10, 20 and 30 wt% of NAP and PVPVA are shown. The exact peak positions for solutions with 10 wt% NAP can be found in Table S3 in Supplementary information. For the alcoholic solvents (Fig 7A to C), a shoulder in the peak of VP carbonyl stretching vibration signal became visible for the solution containing 20 wt% NAP and became more evident for the one with 30 wt% NAP. This signal originated from the sum of aromatic skeleton stretching of NAP and strong hydrogen bonding between NAP and PVPVA[23,25]. For ACN and DCM, this vibration signal was already clearly detected at 1636 cm^{-1} for 10 wt% of NAP (Fig 7D, E). Moreover, in ACN and DCM, the relative intensity of the VA and VP carbonyl stretching region changed when increasing the NAP drug loading, with a similar intensity of both signals for the highest drug loading of 30 wt%.

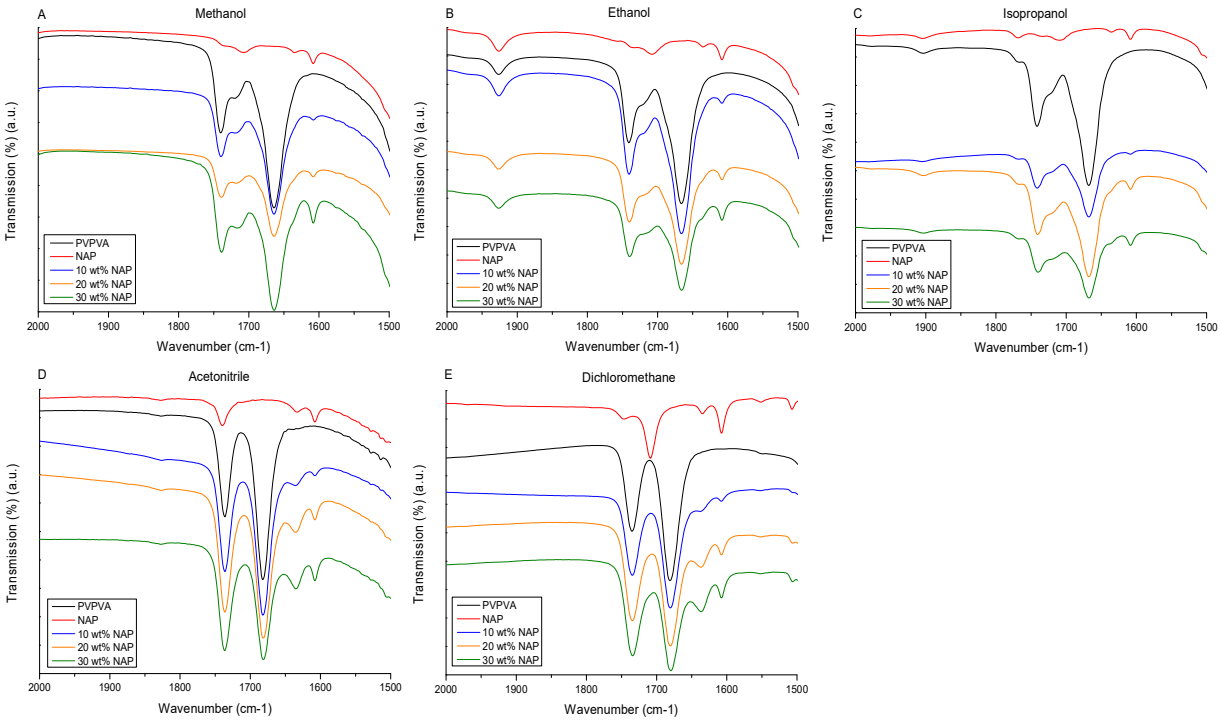

Figure 7*. FT-IR spectra of NAP, PVPVA and 10, 20 and 30 wt% NAP and PVPVA in MeOH (A), EtOH (B), PrOH (C), ACN (D) and DCM (E). The following color code was applied: NAP in red, PVPVA in black, 10 wt% NAP in blue, 20 wt% NAP in orange and 30 wt% NAP in green. The transmittance is depicted in arbitrary units.*

3.2.3. The presence of interactions between FNB and PVPVA in solution

The IR spectra of solutions containing 10, 20 and 30 wt% FNB and PVPVA are depicted in Fig 8 and the corresponding peak positions for the 10 wt% FNB solutions are described in Table S4 in Supplementary information. For the alcoholic solvents, FNB did not influence the behavior of PVPVA in solution (Fig

8A to C). For ACN and DCM, a shoulder peak on the VP carbonyl stretching signal was detected for the solution containing 30 wt% FNB (Fig 8D, E).

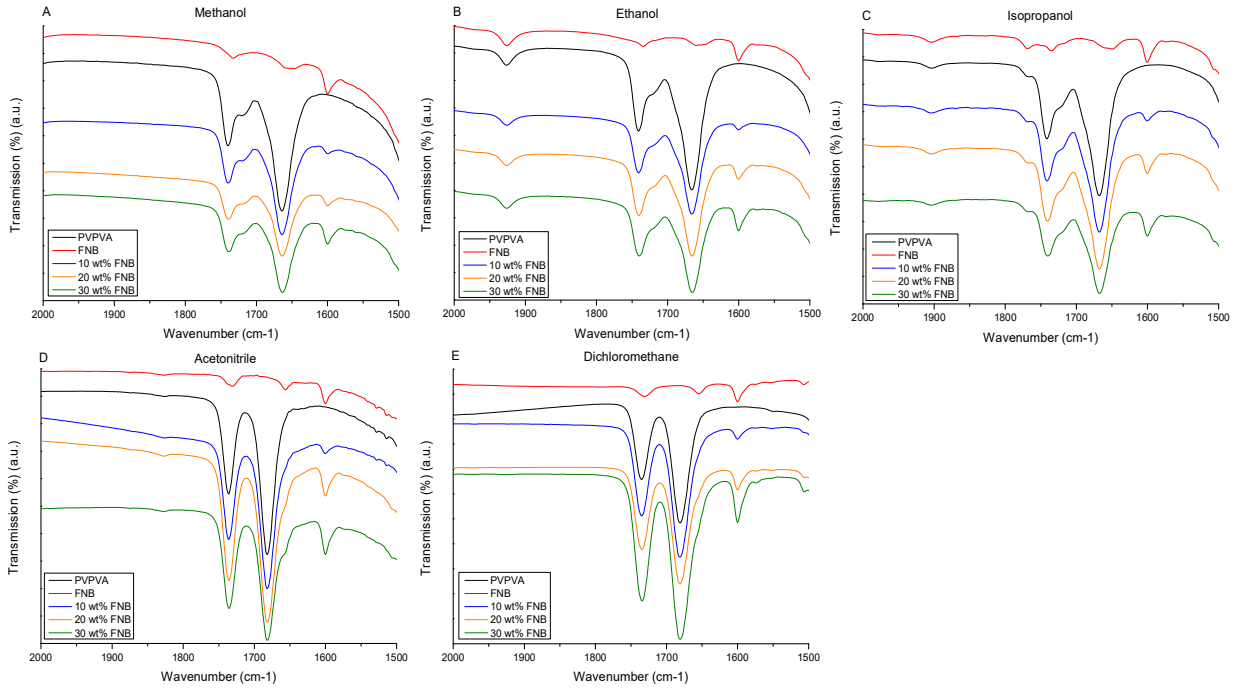

***Figure 8**. FT-IR spectra of FNB, PVPVA and 10, 20 and 30 wt% FNB and PVPVA in MeOH (A), EtOH (B), PrOH (C), ACN (D) and DCM (E). The following color code was applied: FNB in red, PVPVA in black, 10 wt% FNB in blue, 20 wt% FNB in orange and 30 wt% FNB in green. The transmittance is depicted in arbitrary units.*

3.2.4. Comparison of interactions in solution and in the dried state

A comparison of the behavior in solution and dried state of pure PVPVA, pure NAP and samples containing 30 wt% NAP and PVPVA is depicted in Fig 9A and B. The exact peak positions can be found in Table S3 in Supplementary information. In MeOH, the VP carbonyl stretching vibration of PVPVA was broader and positioned at lower wavenumbers and that of its VA group was split in two (Fig 9A). After drying for 1 min at RT, the VA vibration signal was no longer split in two, but positioned at 1733 cm^{-1}, which was in between its signals at 1740 cm^{-1} and 1719 cm^{-1} in solution. Additionally, both carbonyl stretching vibrations appeared broader after drying. Drying of the MeOH solution containing 2% w/V NAP resulted in the formation of both monomer (1732 cm-1) and dimer (1687 cm^{-1}) of NAP. When the solution of both NAP and PVPVA was dried, the shoulder peak on the VP carbonyl stretching vibration that was present in solution became more evident, *i.e.*, the signal at 1636 cm^{-1} in solution was now clearly detected at 1633 cm^{-1}. The relative intensity of the VP and VA carbonyl stretching vibration also changed upon drying, resulting in a similar intensity of both signals. When drying the solution of PVPVA in DCM, only the VP carbonyl stretching vibration was broader and shifted towards lower wavenumbers, *i.e.,* it shifted from 1681 cm^{-1} in solution to 1670 cm^{-1} in dried state (Fig 9B). There was no difference between the IR spectrum of NAP dried from a MeOH solution or from a DCM

solution. Moreover, also the IR spectra from NAP and PVPVA together were identical, thus, there was no longer competition with the solvent for hydrogen bonding, resulting in the formation of hydrogen bonds between NAP and PVPVA, independently of the solvent that was present.

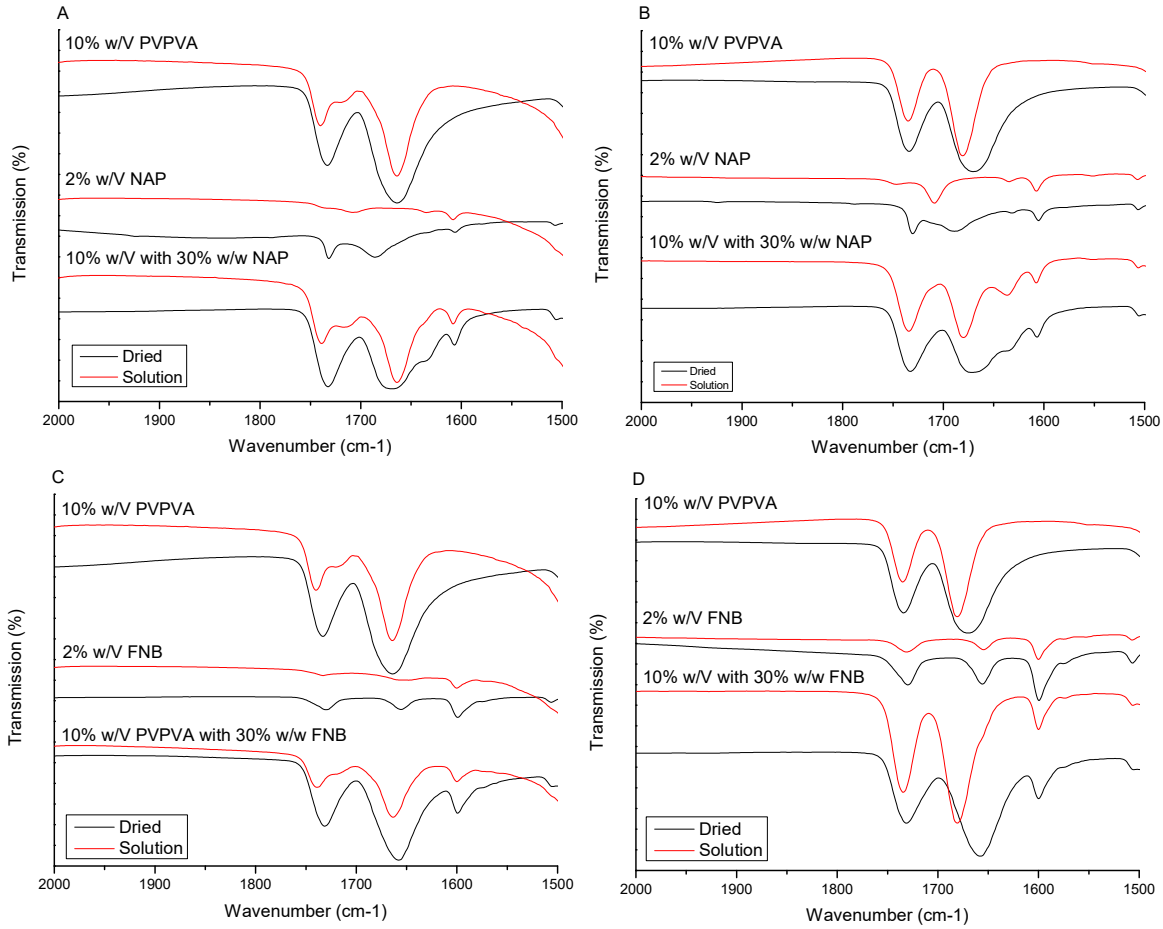

Figure 9. *Comparison of FT-IR spectra in solution to those in the dried state for NAP in/dried from MeOH (A) and DCM (B) and for FNB in/dried from MeOH (C) and DCM (D). The spectra from samples in solutions are depicted in red and those from samples in the dried state in black. The transmittance is shown in arbitrary units.*

Likewise, Fig 9C and D depict the behavior in solution and dried state of pure PVPVA, pure FNB and samples of 30 wt% FNB and PVPVA. The peak positions can be found in Table S4 in Supplementary information. Both in case of MeOH and DCM, the ester carbonyl stretching vibration shifted from 1733 cm^{-1} to 1731 cm^{-1} upon drying of the FNB solution, while the other carbonyl stretching signal was positioned at 1657 cm^{-1} in dried state compared to 1654 cm^{-1} in solution (Fig 9C, D). When drying the solution of both FNB and PVPVA, the carbonyl stretching vibration corresponding to the VP part shifted towards lower wavenumbers, independently of the solvent. More specifically, in case of MeOH, it was positioned at 1657 cm^{-1} in the dried state compared to 1664 cm^{-1} in solution and in the case of DCM, it shifted from 1681 cm^{-1} in solution to 1658 cm^{-1} in dried state. To evaluate the repeatability of the peak shift of the VP carbonyl stretching vibration upon drying, three aliquots of the same solution of 10% w/V PVPVA in DCM were characterized (Fig S1 in Supplementary information). From this, it

403 became clear that the extent of the peak shift upon drying was not repeatable, *i.e.,* vibration bands
404 were detected at 1663 cm^{-1}, 1670 cm^{-1} and 1658 cm^{-1}. Moreover, to investigate possible interactions
405 in the dried state between FNB and PVPVA, ^{13}C-CPMAS ssNMR and liquid state ^{13}C-NMR were applied
406 as well (Fig S2 in Supplementary information). The NMR spectrum of FNB in deuterated chloroform
407 was employed to evaluate peak shifts that might take place upon amorphization of FNB.
408 Characterization of spray dried FNB and PVPVA in 3 different ratios (10 wt%, 20 wt% and 30 wt% FNB)
409 revealed that the only peak shifts present originated from the different physical state of FNB, *i.e.,* the
410 amount of crystalline FNB present.

411 **3.3. Rational selection of spray drying process parameters**

412 Spray drying process parameters were adapted to increase the evaporation rate in the case of MeOH,
413 while in case of DCM, both the influence of an increased and a lower evaporation rate on the physical
414 state was evaluated (Table 1).

415 3.3.1. Spray drying of ASDs of NAP

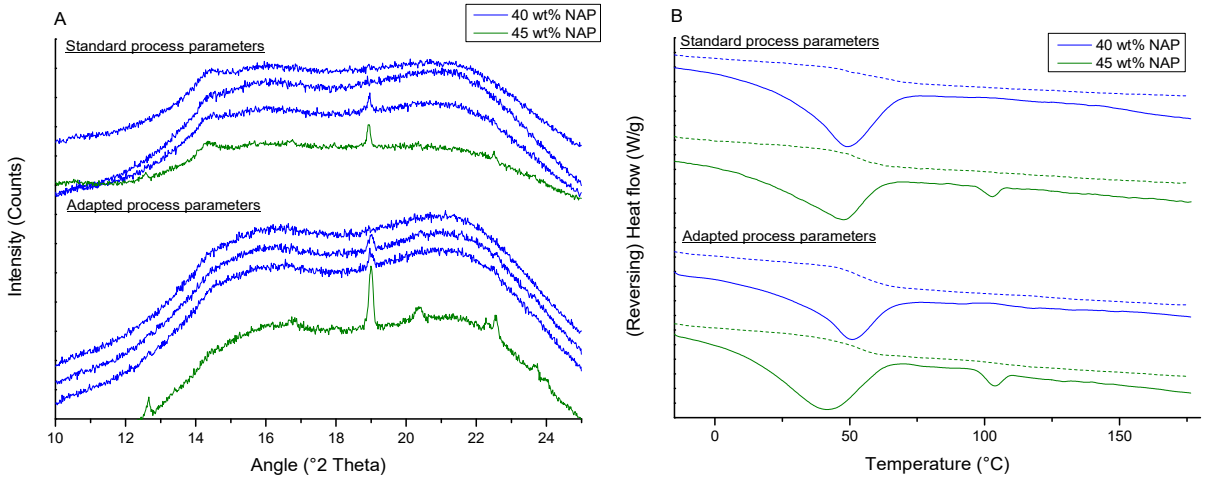

416
417 ***Figure 10****. XRPD diffractograms (A) and mDSC thermograms (B) of 40 wt% (blue) and 45 wt% (green) NAP and PVPVA spray*
418 *dried using MeOH using standard process parameters or parameters that enabled a higher evaporation rate. 40 wt% samples*
419 *were prepared in triplicate (A). For the mDSC analysis, both the reversing (dashed line) and total heat flow (full line) are*
420 *depicted, and exothermic signals are directed upwards (B).*

421 Applying standard process parameters, *i.e*., inlet temperature set at the boiling point of the solvent
422 and a liquid feed rate of 5 mL/min, resulted in a highest drug loading of 40 wt% NAP when using MeOH.
423 When preparing 3 batches with the same composition, one of them was partially crystalline in XRPD
424 analysis (Fig 10A). Likewise, two out of three batches showed Bragg reflections when a higher
425 evaporation rate was applied. Independently of the set of process parameters used, the 45 wt% sample
426 was partially crystalline, although the crystalline fraction was larger in case of the higher evaporation
427 rate, *i.e.,* 2.52 ± 0.17 % compared to 1.76 ± 0.14 % (Fig 10). In spite of this, a lower residual solvent
428 content was found when a higher evaporation rate was applied (Table S5 in Supplementary
429 information).

Using DCM as a solvent and standard process parameters gave rise to a maximum drug loading of 45 wt%, which was determined by the presence of a melting event of NAP in the total heat flow of the mDSC analysis for higher drug loadings (Fig S3 in Supplementary information). Similarly, the thermogram of 50 wt% NAP prepared using a higher evaporation rate also contained a melting event, although the crystalline content was higher, *i.e.,* 1.58 ± 0.09 % compared to 0.29 ± 0.16 %. Interestingly, when applying a lower evaporation rate, there were neither melting events detected in the mDSC analysis for the 50 wt% nor Bragg peaks in the XRPD analysis (Fig S3 in Supplementary information).

3.3.2. Spray drying of ASDs of FNB

When using MeOH with standard process parameters, Bragg peaks were present in the XRPD diffractogram starting from 10 wt% FNB (Fig 11A). Adapting the parameters to increase the drying rate, resulted in an amorphous halo for 10 wt% FNB, yet for the 15 wt% FNB Bragg reflections could be detected at 16, 17 and 22° °2θ (Fig 11B). According to the TGA-analysis, a higher evaporation rate resulted in a lower amount of residual solvent in the 5 wt% FNB batches, *i.e.,* 2.73 ± 0.18 % compared to 4.05 ± 0.25 % (Table S6 in Supplementary information).

When spray drying with DCM, the highest drug loading of FNB that could be kinetically stabilized was previously established at 20 wt% [5]. Applying a lower evaporation rate resulted in a partially crystalline sample for the 20 wt% (Fig S4 in Supplementary information). Increasing the evaporation rate on the other hand, resulted in an X-ray amorphous 20 and 25 wt% FNB sample, while Bragg peaks were present for the 30 wt% FNB one.

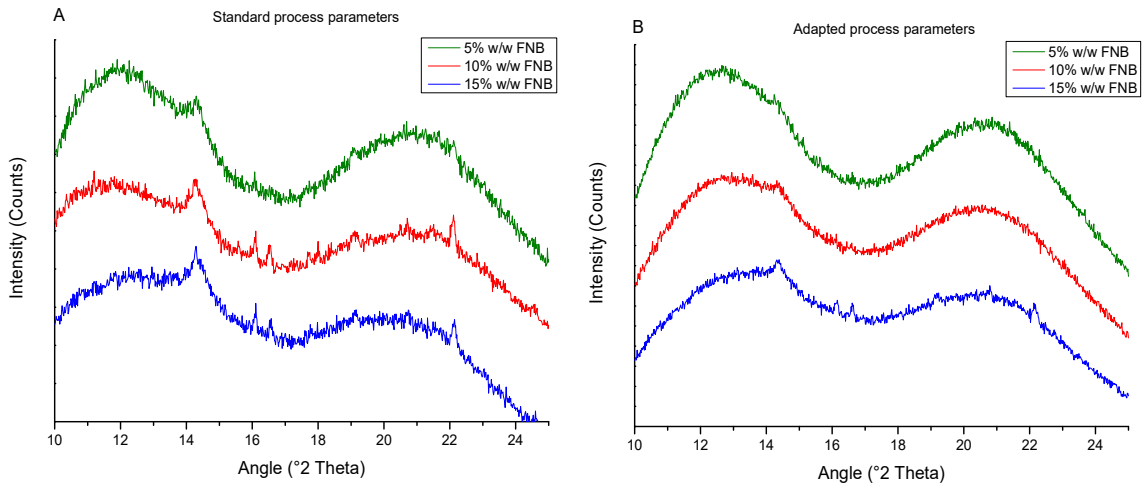

Figure 11. *XRPD diffractograms of 5 wt% (green), 10 wt% (red) and 15 wt% (blue) FNB and PVPVA spray dried using MeOH with standard process parameters (A) and parameters that allowed a faster evaporation of MeOH (B).*

4. Discussion

4.1. Evaporation kinetics

The pure organic solvents exhibited a different evaporation rate in spite of the similar energy input relative to the bp of the solvents (Fig 3). This difference could however not be related to the purity of the solvents. For instance, the effect of residual water was investigated by analyzing purer MeOH (99.9%), which still had a lower evaporation rate compared to EtOH (97%) (data not shown).

Addition of PVPVA did not alter the relative evaporation rate of these seven solvents, yet it decreased the evaporation rate in all cases (except for PrOH) (Fig 3, 4A). This could be explained by the lower vapor pressure of the solutions compared to their pure counterparts, which was responsible for a lower tendency to evaporate and hence a slower evaporation process. Moreover, during evaporation, the PVPVA concentration increased, resulting in an increased viscosity, which in turn also decreased the evaporation rate. The latter was most pronounced for the faster evaporating solvents, *i.e*. DCM, Ac and EtAc, where a very fast increase in PVPVA concentration and thereby the viscosity of the solution gave rise to what could be considered as skin formation through which further solvent evaporation had to take place. The different impact of PVPVA on the evaporation behavior of relatively faster and slower evaporating solvents was confirmed by determining the evaporation kinetics of MeOH and DCM solutions containing 30% w/V PVPVA (Fig 5). Here, the delaying effect of PVPVA was much more pronounced in case of DCM yet, it was also present in the case of MeOH at later timepoints, which demonstrated that in both cases skin formation took place, it only took a longer period of time in the case of the initially slower evaporating solvent. The different effect of PVPVA on the drying rate of organic solvents might also have implications for the particle morphology. For instance, it has been described by Boel et al. that the difference in evaporation rate of MeOH and Ac during fluid bed coating was responsible for the morphology of bead coated ASDs of felodipine, where a porous coating was observed for the faster evaporating Ac compared to a homogeneous coating for the slower evaporating MeOH[27]. However, microscopic evaluation of PVPVA particles spray dried with the seven different solvents revealed that all were collapsed (except for PrOH), hence, the difference in evaporation behavior could not be directly related to the morphology of spray dried PVPVA particles (data not shown).

When part of the PVPVA was replaced with an API, which was either FNB or NAP, the initial evaporation rate was higher in the case of DCM, Ac and EtAc, which could be explained by a less pronounced viscosity increase during evaporation in the presence of the APIs compared to pure PVPVA, which would in turn lead to less rapid skin formation. Further in time, in the presence of FNB, all solvents

evaporated faster compared to pure PVPVA, while in the presence of NAP all solvents showed a slower evaporation process (except for DCM)(Fig 4B, C). These results could be an indication of interactions between both NAP and the solvent and NAP and PVPVA, as the latter could result in a viscosity increase and thereby a lower evaporation rate as well. On the other hand, it might indicate the absence of/weaker interactions between both FNB and the solvent and FNB and PVPVA.

4.2. FT-IR spectroscopy

The IR spectra of PVPVA in solution revealed the formation of hydrogen bonds between PVPVA and the alcoholic solvents (Fig 6A). The VP carbonyl stretching vibration was broadened and shifted towards lower wavenumbers, while the VA carbonyl stretching vibration was split in two vibration bands. The VP amide carbonyl accepted protons thus more readily compared to the VA ester carbonyl, which could be attributed to the more polar nature of the VP part of the copolymer and its well-known availability for hydrogen bonding[28]. Additionally, the extent of the peak shift of the VP carbonyl stretching vibration was dependent on the alcoholic solvent, demonstrating that stronger hydrogen bonds were formed between PVPVA and MeOH than between PVPVA and EtOH and those were in turn stronger than the ones between PVPVA and PrOH (Fig 6A).

Also NAP interacted differently with MeOH, EtOH, PrOH, ACN and DCM (Fig 6B). In the alcoholic solvents and in DCM, NAP existed as both dimer and monomer, although there was relatively more dimer formed in DCM[16]. As previously reported in literature, there was no dimer formation observed in the weakly hydrogen bond accepting solvent ACN (Fig 6B)[24]. The sole presence of the monomer at 1740 cm^{-1} demonstrated that NAP was more available for interaction with the solvent when compared to the other solvents. From this different self-association behavior of NAP, it could be concluded that NAP interacted the strongest with ACN, followed by all three alcoholic solvents and it had the weakest interactions with DCM.

When NAP and PVPVA were dissolved together, the presence of the shoulder peak on the VP carbonyl stretching vibration indicated strong hydrogen bonding between NAP and PVPVA (Fig 7). This shoulder peak was detected from 20 wt% NAP in the alcoholic solvents, while it was already detected from 10 wt% NAP in case of ACN and DCM, demonstrating that NAP and PVPVA formed stronger hydrogen bonds in ACN and DCM. This could be attributed to the multiple interaction possibilities in the alcoholic solvents: hydrogen bonding was not only possible with PVPVA, but also with NAP, resulting in less free PVPVA and NAP to associate with each other. Therefore, the tendency for NAP and PVPVA to hydrogen bond with one another was higher in case of DCM and ACN compared to the other solvents. This is an important finding as these results clearly indicate that the probability of API-polymer interactions is influenced by the solvent, which might have implications for the formulation of highly drug loaded

519 ASDs and/or the physical stability of ASDs. Interestingly, there was no difference observed in API-
520 polymer interactions between ACN and DCM, although the self-association behavior of NAP in these
521 solvents was clearly different (Fig 7D, E). This demonstrated that the affinity of NAP for PVPVA, a strong
522 hydrogen acceptor, was higher than for ACN, a weak hydrogen acceptor.

523 When the IR spectra of NAP and PVPVA in solution were compared to those in the dried state (Fig 9A
524 and B), it was evident that after drying, there was no longer competition with the solvent for hydrogen
525 bonding, resulting in the formation of hydrogen bonds between NAP and PVPVA, independently of the
526 solvent. Thus, although the prevalence of interactions between NAP and PVPVA was much higher in
527 case of DCM compared to MeOH, this did not influence the interactions formed upon drying.
528 Additionally, widening of the carbonyl stretching vibrations of PVPVA was observed, and especially
529 that of the VP, originated from water uptake from the environment when drying at RT for 1 min. This
530 was most pronounced for the VP carbonyl stretching vibration due to the hygroscopic nature of VP[29].

531 In the case of FNB, the broadening of the second carbonyl stretching vibration in MeOH, EtOH and
532 PrOH indicated that FNB could hydrogen bond with these solvents (Fig 6C). The IR spectra of FNB
533 together with PVPVA were an overlap of the spectra of the individual components in solution,
534 indicating that there were no interactions between FNB and PVPVA (Fig 8). The shoulder peak present
535 on the VP carbonyl stretching vibration in ACN and DCM was not detected in case of the alcoholic
536 solvents because of the peak positioning of the VP signal (*i.e.,* shifted towards lower wavenumbers),
537 its broadening and the broadening of the carbonyl stretching vibration of FNB. In conclusion, there
538 were no interactions observed between FNB and PVPVA, independently of the solvent. In the dried
539 state, there was a large shift of the VP carbonyl stretching vibrations towards lower wavenumbers,
540 which appeared to be dependent on the solvent (Fig 9C, D). Further investigation of these spectral
541 changes revealed that this peak shift was not repeatable, which could be explained by a variable water
542 uptake from the environment upon drying, which gave in turn rise to a different level of hydrogen
543 bonding. Additionally, the absence of interactions between FNB and PVPVA in the solid state was
544 confirmed by the application of ^{13}C-CPMAS ssNMR.

545 **4.3. Correlation between evaporation rate and interactions in solution**

546 The evaporation behavior of solutions containing both PVPVA and an API was influenced by the API:
547 the evaporation rate constants of the 30 wt% FNB solutions were highest, followed by the 100 wt%
548 PVPVA solutions and the ones of the 30 wt% NAP solutions were the lowest (Fig 4B). In spite of the fact
549 that both PVPVA and FNB could hydrogen bond with the alcoholic solvents (Fig 6A, C), alcoholic
550 solutions containing FNB and PVPVA evaporated faster compared to the ones of PVPVA alone, which
551 could be explained by a lower affinity of these protic solvents for FNB compared to PVPVA and/or a

lower viscosity of the solutions containing both FNB and PVPVA. On the other hand, it was found that NAP could hydrogen bond with MeOH, EtOH, PrOH and ACN (Fig 6B), which could be a possible explanation for the lower tendency to evaporate in presence of NAP, on the condition that the affinity of these solvents for NAP was higher than for PVPVA. Also the hydrogen accepting solvents Ac and EtAc could potentially interact with NAP, however, this could not be established by FT-IR because of overlap of the vibration bands of these solvents with those of NAP and PVPVA in the spectral region of interest. Another explanation for the slower evaporation process in presence of NAP could be the formation of hydrogen bonds between NAP and PVPVA (Fig 7), which could give rise to an increased viscosity of the solution. In spite of the fact that the prevalence of interactions between API-polymer-solvent could explain the differences in evaporation behavior during these TGA-experiments, the relevance of these differences for the final phase behavior of ASDs was not yet fully elucidated and could be interesting subject for further investigations.

4.4. Correlation between evaporation rate and phase behavior of ASDs

As the evaporation behavior was studied to gain insight in the contribution of the solvent to the phase behavior of spray dried ASDs immediately after production, the relation between the evaporation rate constants of 10% w/V PVPVA solutions and the highest drug loadings of FNB and NAP obtained by spray drying is depicted in Fig 12. Moreover, the difference in outlet temperature (T_{out}), *i.e.,* the difference between the T_{out} in the beginning of the process and that at the end of the process, observed during spray drying of 10% w/V PVPVA solutions is shown as well. The values of these highest drug loadings and T_{out}*s* were reported in previous work[5]. The larger the difference in T_{out} was, the more energy consuming the drying process was, thus, the energy requirement to evaporate MeOH was highest under these circumstances. Interestingly, the difference in T_{out} was inversely related to the highest drug loadings of FNB and NAP that could be obtained, hence, the more energy consuming a process was, the lower the drug loading that could be kinetically stabilized in the polymer matrix. This could be (at least partially) related to the evaporation rate constants deducted from the TGA-experiments. Generally, the higher the evaporation rate, the less energy consuming the process was and the higher the maximum drug loading was. However, while DCM evaporated the fastest at 10 °C below its bp, the amount of energy required to evaporate DCM during spray drying was higher compared to Ac and EtAc, and consequently the highest drug loadings that could be achieved were also lower when DCM was used. The TGA- experiments do not account for a difference in droplet size distribution during spray drying. Hence, in spite of the fact that the liquid feed rate was adapted to the solvent, it is possible that the same feed rate gave rise to a difference in droplet size distribution when another solvent was used. Accordingly, a possible explanation for the higher energy requirement in case of DCM is the generation of larger droplets. Although the TGA-experiments gave a good indication

of the difference in evaporation kinetics of the organic solvents and the influence of solutes on their drying behavior, it does not account for all factors that determine the drying process in a spray drying set-up.

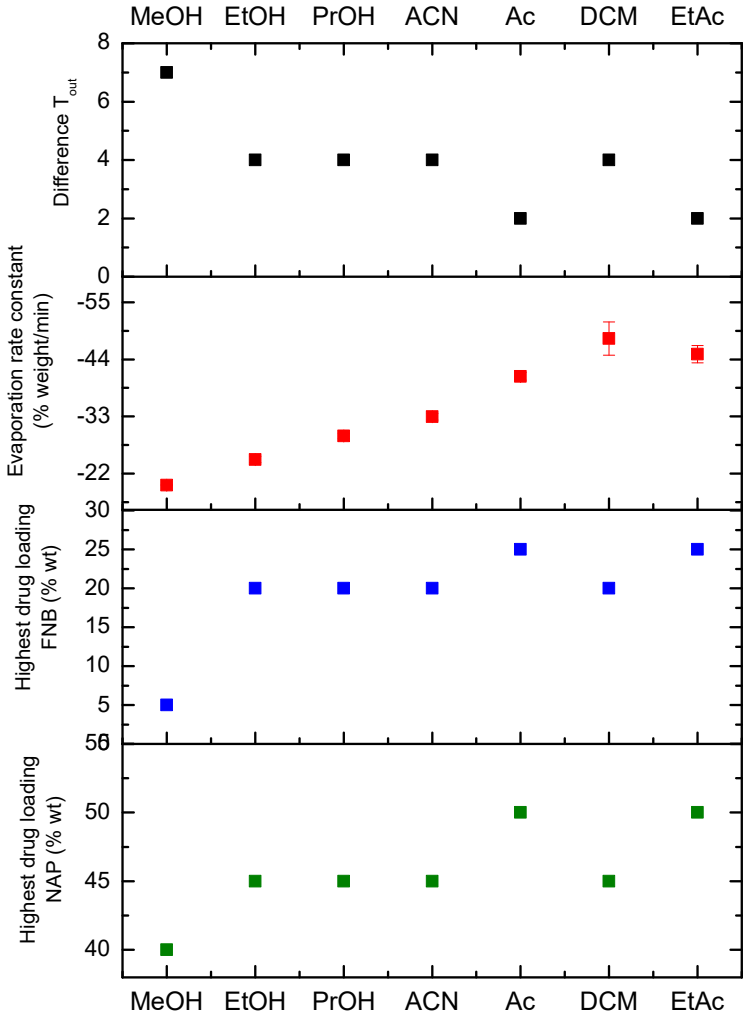

Figure 12. *Difference in T_{out} observed during spray drying of 10% w/V PVPVA solutions (black), evaporation rate constants (%weight/min) of 10% w/V PVPVA solutions deducted using a linear fit (red), and highest drug loadings of FNB (blue) and NAP (green) obtained by spray drying. Every factor is shown per solvent.*

4.5. Rational selection of spray drying process parameters

As MeOH had the lowest evaporation rate, formed the strongest hydrogen bonds with PVPVA and it could also interact with both FNB and NAP, it had the poorest properties to formulate highly drug loaded ASDs. In contrast to this, DCM evaporated the fastest and there were no interactions observed between either the drugs and DCM or PVPVA and DCM, which made DCM a promising solvent to be used to prepare highly drug loaded ASDs. Accordingly, the influence of adapting spray drying process parameters on the highest drug loading that could be kinetically stabilized was explored for these two extremes (Table 2).

It was found that ASDs of 40 wt% NAP and PVPVA were one out of three times partially crystalline when using standard process parameters with MeOH, compared to two out of three when increasing the drying rate (Fig 10). The phase behavior was thus not repeatable, which could be attributed to variables, such as environmental conditions (*i.e.,* RH and T) that cannot be controlled in a spray drying set-up. More importantly, increasing the drying rate of MeOH resulted in poorer phase behavior and hence, it did not allow the formulation of higher drug loadings of NAP. These findings were in contrast with the idea that faster solvent evaporation would be favorable for kinetic trapping and thus the formulation of kinetically stabilized highly drug loaded ASDs.

However, not only the evaporation rate, but also the T_{out} is a very critical factor for the phase behavior of a spray dried ASD. In Table 2, both the T_{out} in the beginning and the end of the spray drying process are reported. The larger the difference between these values, the more energy consuming the drying process was, *e.g.,* a ΔT of 2 °C in case of process parameters that enabled a higher evaporation rate relative to a ΔT of 5 °C for standard process parameters. Moreover, the crystallization rate increases when the difference between the T_g of the ASD and the particle temperature (and thus T_{out}) increases[2,30]. To exemplify, as the T_g of 40 wt% NAP and PVPVA ASDs was ca. 55.52 °C, installing an inlet temperature (T_{in}) of 85 °C when spray drying with MeOH gave rise to a T_{out} situated above the T_g (Table 2). This increased crystallization tendency together with the fact that NAP is a very fast crystallizer, classified as a Glass Forming Ability (GFA) Class I compound according to Van Eerdenbrugh et al., resulted in a poorer phase behavior when applying process parameters that enabled a faster evaporation process[31]. On the other hand, installing a lower T_{in} when spray drying with DCM, gave rise to a T_{out} situated further below the T_g of ASDs of NAP than when applying standard parameters, *i.e.,* ASDs of 45 wt% NAP and PVPVA had a T_g of ca. 51.60 °C relative to a T_{out} of 28 °C. Hence, lowering the drying rate indirectly decreased the crystallization tendency. Likewise, Paudel et al. investigated the effect of the T_{in} on the phase behavior of ASDs of NAP and PVP K25, where higher T_{in}*s* resulted in phase separated systems[20]. Ultimately, the drying air temperature should be sufficiently high to remove the solvent and enable kinetic trapping of the drug in the polymer matrix, yet it should be in balance with the potentially unfavorable impact of a high T_{out} on the crystallization tendency.

The fact that an increased drying air temperature had a disadvantageous effect on the phase behavior of ASDs of NAP, does not exclude the possible beneficial effect of an increased drying rate on the kinetic trapping efficiency. For instance, solely modifying the liquid feed rate to generate smaller droplets could still result in a faster evaporation process without increasing the T_{out}. Therefore, a further process optimization might give rise to the kinetic stabilization of higher drug loadings.

Table 2. *Outlet temperatures (T_{out}) observed during spray drying of ASDs of 40 wt% NAP and PVPVA using MeOH and ASDs of 45 wt% NAP and PVPVA using DCM.*

Solvent	Condition	T_{in} (°C)	$T_{out, begin}$ (°C)	$T_{out, end}$ (°C)	ΔT_{out} (°C)
MeOH	Standard evaporation rate	65	48	43	5
	Higher evaporation rate	85	60	58	2
DCM	Standard evaporation rate	39	33	28	5
	Higher evaporation rate	59	44	42	2
	Lower evaporation rate	29	28	22	6

In contrast, increasing the drying rate did allow the formulation of higher drug loadings for ASDs of FNB, both in case of MeOH and DCM. Lowering the evaporation rate of DCM on the other hand, gave rise to poorer phase behavior compared to the standard evaporation rate. These findings were in accordance with the expected favorable effect of an increased evaporation rate on the kinetic trapping efficiency and thereby formulation of highly drug loaded ASDs. The absence of a disadvantageous effect of the higher T_{out} can be explained by the lower drug loadings of FNB that were prepared, namely 5 to 30 wt%, and thus higher product T_g, *i.e.,* ranging from 100 °C for 5 wt% FNB to 54.50 °C for 30 wt% FNB[5]. In spite of that, a possible explanation for the partial crystallinity of the 30 wt% FNB sample when increasing the drying rate of DCM, could be the relatively higher T_{out} of 44 °C (Table S7 in Supplementary information). However, the physical state of these ASDs of FNB was predominantly determined by the increased drying rate (T_{in}) rather than the T_{out} as was the case for ASDs of NAP. Evidently, depending on the physicochemical characteristics of the API (*e.g.,* GFA) and the API to polymer ratio, the T_{out} will be a limiting factor for increasing evaporation rate by adaptation of the T_{in}.

In spite of the fact that a higher amount of FNB could be kinetically stabilized by increasing the drying rate, the improvement was limited to 5 wt%, independently of the solvent. Especially for MeOH, this cannot be related to the T_{out}, as an ASD of 10 wt% FNB had a T_g of ca. 93.29 °C, which is well above the T_{out} of 60 °C. Accordingly, the physical state was not only determined by the balance of T_{in} and T_{out}, but more importantly, by the API-polymer-solvent combination. For MeOH, this could be related to the inherently slow evaporation behavior of the solvent relative to the others (even when applying parameters that enable a higher drying rate) together with the fact that MeOH can hydrogen bond with both PVPVA and FNB. Ultimately, the physical state of these ASDs of FNB immediately after production was determined by the API-polymer-solvent combination rather than the set of spray drying process parameters used.

5. Conclusion

The combination of TGA and FT-IR spectroscopy was successfully applied to gain insight in the evaporation kinetics and interactions (in solution), respectively. The evaporation rate of the seven organic solvents 10 °C below the bp of the respective solvent clearly differed, with MeOH evaporation the slowest and DCM the fastest. The addition of PVPVA did not alter the relative evaporation rate, yet decreased the evaporation rate for all solvents, which was most pronounced for the relatively faster evaporating solvents, *i.e.,* DCM, Ac and EtAc. FNB and NAP had opposite effects on the evaporation rate: FNB increased the drying rate again, while NAP decreased it. The latter was an indication of interactions between NAP and PVPVA or NAP and the solvent. Accordingly, the FT-IR analyses revealed hydrogen bonding between NAP and MeOH, EtOH, PrOH and ACN, and hydrogen bonding between NAP and PVPVA, which was more pronounced for the solvents that did not interact with PVPVA, *i.e.,* DCM and ACN. However, drying from DCM or MeOH resulted in the same IR spectrum of NAP and PVPVA, demonstrating that the same hydrogen bonding strength could still be obtained. Based on these findings, spray drying process parameters were altered to increase the evaporation rate of MeOH and to both lower and increase the drying rate of DCM. For FNB, a higher evaporation rate enabled the formulation of higher drug loadings, which was in line with the idea that an increased drying rate favored kinetic trapping and thereby the formulation of supersaturated ASDs. On the other hand, an increased drying rate did result in poorer phase behavior of ASDs of NAP, while a lower evaporation rate allowed the kinetic stabilization of higher drug loadings. These findings could be related to the relative position of the T_g of the ASD to the T_{out}, where the crystallization tendency was increased due to the smaller temperature difference. Hence, the drying air temperature should be high enough to enable kinetic trapping, but in balance with the potentially unfavorable impact of a high T_{out} on the crystallization tendency. Moreover, even when higher drug loadings could be kinetically stabilized by altering the process parameters, the improvement was limited. Hence, the phase behavior of these ASDs of FNB and NAP immediately after production was predominantly determined by the API-polymer-solvent combination rather than the process parameters applied.

Acknowledgements

The authors would like to thank Fonds Wetenschappelijk Onderzoek Vlaanderen (FWO) and Laboratoires SMB for their support. Danny Winant (Materials Engineering, KU Leuven), Jasper Beyens (Pharmaceutical Analysis, KU Leuven) and Gunther Reekmans (Chemistry department, Hasselt University) are acknowledged for technical assistance. P.A. also wants to thank Hasselt University and the Research Foundation Flanders (FWO) for the Hercules project AUHL/15/2—GOH3816N.

Supporting information

Table S1 – S4: Peak positions of vibration bands as determined by FT-IR spectroscopy.

Table S5 – S6: Residual solvent after spray drying of ASDs of FNB or NAP.

Table S7: Outlet temperatures observed during spray drying of ASDs of FNB.

Fig S1: FT-IR spectra of PVPVA after drying for 1 min at RT from a solution of 10% w/V PVPVA in DCM.

Fig S2: ^{13}C-NMR spectra of spray dried ASDs of FNB.

Fig S3 – S4: Solid-state characterization of ASDs of NAP or FNB spray dried using DCM.

References

1. Chiou WL, Riegelman S. Pharmaceutical Applications of Solid Dispersion Systems. *J Pharm Sci*. 1971;60(9):1281-1302. doi:10.1002/jps.2600600902

2. Singh A, Van den Mooter G. Spray drying formulation of amorphous solid dispersions. *Adv Drug Deliv Rev*. 2016;100:27-50. doi:10.1016/j.addr.2015.12.010

3. Wu JX, Yang M, Berg F Van Den, Pajander J, Rades T, Rantanen J. Influence of solvent evaporation rate and formulation factors on solid dispersion physical stability. *Eur J Pharm Sci*. 2011;44(5):610-620. doi:10.1016/j.ejps.2011.10.008

4. Paudel A, Worku ZA, Meeus J, Guns S, Van den Mooter G. Manufacturing of solid dispersions of poorly water soluble drugs by spray drying: Formulation and process considerations. *Int J Pharm*. 2013;453(1):253-284. doi:10.1016/j.ijpharm.2012.07.015

5. Dedroog S, Boel E, Kindts C, Appeltans B, Van den Mooter G. The underestimated contribution of the solvent to the phase behavior of highly drug loaded amorphous solid dispersions. *Int J Pharm*. Published online 2021:121201. doi:10.1016/j.ijpharm.2021.121201

6. Al-Obaidi H, Brocchini S, Buckton G. Anomalous properties of spray dried solid dispersions. *J Pharm Sci*. 2009;98:4757-4737. doi:10.1002/jps

7. Defrese MK, Farmer MA, Long Y, Timmerman LR, Bae Y, Marsac PJ. Approaches to Understanding the Solution-State Organization of Spray-Dried Dispersion Feed Solutions and Its Translation to the Solid State. *Mol Pharm*. 2020;17(12):4548-4563. doi:10.1021/acs.molpharmaceut.0c00729

8. Hugo M, Kunath K, Dressman J. Selection of excipient, solvent and packaging to optimize the performance of spray-dried formulations: Case example fenofibrate. *Drug Dev Ind Pharm*. 2013;39(2):402-412. doi:10.3109/03639045.2012.685176

9. Paudel A, Van den Mooter G. Influence of solvent composition on the miscibility and physical stability of naproxen/PVP K 25 solid dispersions prepared by cosolvent spray-drying. *Pharm Res*. 2012;29(1):251-270. doi:10.1007/s11095-011-0539-x

10. Thakore SD, Prasad R, Dalvi S V., Bansal AK. Role of solvent in differential phase behavior of celecoxib during spray drying. *Int J Pharm*. 2020;585(May):119489. doi:10.1016/j.ijpharm.2020.119489

11. Wan F, Bohr A, Jonas Maltesen M, et al. Critical Solvent Properties Affecting the Particle Formation Process and Characteristics of Celecoxib-Loaded PLGA Microparticles via Spray-Drying. *Pharm Res*. 2013;30:1065-1076. doi:10.1007/s11095-012-0943-x

12. Mugheirbi NA, Mosquera-Giraldo LI, Borca CH, Slipchenko L V., Taylor LS. Phase Behavior of Drug-Hydroxypropyl Methylcellulose Amorphous Solid Dispersions Produced from Various Solvent Systems: Mechanistic Understanding of the Role of Polymer using Experimental and Theoretical Methods. *Mol Pharm*. 2018;15(8):3236-3251. doi:10.1021/acs.molpharmaceut.8b00324

13. Taylor LS, Li N, Cape JL, et al. Water-induced phase separation of spray-dried amorphous solid dispersions. *Mol Pharm*. 2020;17(10):4004-4017. doi:10.1021/acs.molpharmaceut.0c00798

14. Vehring R, Foss WR, Lechuga-Ballesteros D. Particle formation in spray drying. *J Aerosol Sci*. 2007;38(7):728-746. doi:10.1016/j.jaerosci.2007.04.005

15. Boel E, Koekoekx R, Dedroog S, et al. Unraveling particle formation: From single droplet drying

to spray drying and electrospraying. *Pharmaceutics*. 2020;12(7):1-58. doi:10.3390/pharmaceutics12070625

16. Velazquez MM, Valero M, Rodríguez LJ, Costa SMB, Santos MA. Hydrogen bonding in a non-steroidal anti-inflammatory drug-Naproxen. *J Photochem Photobiol B Biol*. 1995;29(1):23-31. doi:10.1016/1011-1344(95)90245-7

17. Jubert A, Legarto ML, Massa NE, Tévez LL, Okulik NB. Vibrational and theoretical studies of non-steroidal anti-inflammatory drugs Ibuprofen [2-(4-isobutylphenyl)propionic acid]; Naproxen [6-methoxy-α-methyl-2-naphthalene acetic acid] and Tolmetin acids [1-methyl-5-(4-methylbenzoyl)-1H-pyrrole-2-acetic acid]. *J Mol Struct*. 2006;783(1-3):34-51. doi:10.1016/j.molstruc.2005.08.018

18. Yani Y, Kanaujia P, Chow PS, Tan RBH. Effect of API-Polymer Miscibility and Interaction on the Stabilization of Amorphous Solid Dispersion: A Molecular Simulation Study. *Ind Eng Chem Res*. 2017;56(44):12698-12707. doi:10.1021/acs.iecr.7b03187

19. Ziaee A, Albadarin AB, Padrela L, Faucher A, O'Reilly E, Walker G. Spray drying ternary amorphous solid dispersions of ibuprofen – An investigation into critical formulation and processing parameters. *Eur J Pharm Biopharm*. 2017;120(May):43-51. doi:10.1016/j.ejpb.2017.08.005

20. Paudel A, Loyson Y, Guy V den M. An Investigation into the Effect of Spray Drying Temperature and Atomizing Conditions on Miscibility, Physical Stability, and Performance of Naproxen–PVP K 25 Solid Dispersions. *J Pharm Sci*. 2013;102:1249-1267. doi:10.1002/jps

21. Patel AD, Agrawal A, Dave RH. Investigation of the effects of process variables on derived properties of spray dried solid-dispersions using polymer based response surface model and ensemble artificial neural network models. *Eur J Pharm Biopharm*. 2014;86(3):404-417. doi:10.1016/j.ejpb.2013.10.014

22. Chiu CY, Yen YJ, Kuo SW, Chen HW, Chang FC. Complicated phase behavior and ionic conductivities of PVP-co-PMMA-based polymer electrolytes. *Polymer (Guildf)*. 2007;48(5):1329-1342. doi:10.1016/j.polymer.2006.12.059

23. Worku ZA, Aarts J, Singh A, Van Den Mooter G. Drug-polymer miscibility across a spray dryer: A case study of naproxen and miconazole solid dispersions. *Mol Pharm*. 2014;11(4):1094-1101. doi:10.1021/mp4003943

24. Tomasko DL, Timko MT. Tailoring of specific interactions to modify the morphology of naproxen. *J Cryst Growth*. 1999;205(1):233-243. doi:10.1016/S0022-0248(99)00237-7

25. Paudel A, Nies E, Van den Mooter G. Relating hydrogen-bonding interactions with the phase behavior of naproxen/PVP K 25 solid dispersions: Evaluation of solution-cast and quench-cooled films. *Mol Pharm*. 2012;9(11):3301-3317. doi:10.1021/mp3003495

26. Sailaja U, Thayyil MS, Kumar NSK, Govindaraj G. Molecular dynamics of amorphous pharmaceutical fenofibrate studied by broadband dielectric spectroscopy. *J Pharm Anal*. 2016;6(3):165-170. doi:10.1016/j.jpha.2014.09.003

27. Boel E, Giacomini F, Van den Mooter G. Solvent influence on manufacturability, phase behavior and morphology of amorphous solid dispersions prepared via bead coating. *Eur J Pharm Biopharm*. 2021;167(May):175-188. doi:10.1016/j.ejpb.2021.07.013

28. Joo SH, Kim JH, Kang SW, Jang J, Kang YS. Propylene sorption and coordinative interactions for poly(N-vinyl pyrrolidone-co-vinyl acetate)/silver salt complex membranes. *J Polym Sci Part B Polym Phys*. 2007;45(16):2263-2269. doi:10.1002/polb.21244

790 29. Taylor LS, Langkilde FW, Zografi G. Fourier transform Raman spectroscopic study of the
791 interaction of water vapor with amorphous polymers. *J Pharm Sci*. 2001;90(7):888-901.
792 doi:10.1002/jps.1041

793 30. Islam MIU, Langrish TAG. An investigation into lactose crystallization under high temperature
794 conditions during spray drying. *Food Res Int*. 2010;43(1):46-56.
795 doi:10.1016/j.foodres.2009.08.010

796 31. Van Eerdenbrugh B, Raina S, Hsieh Y-L, Augustijns P, Taylor LS. Classification of the
797 Crystallization Behavior of Amorphous Active Pharmaceutical Ingredients in Aqueous
798 Environments. *Pharm Res*. 2014;31(4):969-982. doi:10.1007/s11095-013-1216-z

799